

UC Irvine

UC Irvine Electronic Theses and Dissertations

Title

Electrodeposition of Cobalt and Nickel for Hydrometallurgical Lithium Ion Battery Recycling

Permalink

<https://escholarship.org/uc/item/4ms1p1nh>

Author

Reyes, Anthony Castillo

Publication Date

2023

Peer reviewed|Thesis/dissertation

**UNIVERSITY OF CALIFORNIA,
IRVINE**

Electrodeposition of Cobalt and Nickel for Hydrometallurgical Lithium Ion Battery Recycling

THESIS

submitted in partial satisfaction of the requirements for the degree of

MASTER OF SCIENCE

in Engineering, Concentration in Materials and Manufacturing Technology

by

Anthony Castillo Reyes

Thesis Committee:

Associate Professor Iryna Zenyuk, Chair

Distinguished Professor Diran Apelian

Professor Daniel Mumm

2023

Copyright

Dedication

To my cousins, Shangrila and Christine

and my girlfriend Sydney

for their support when needed most

Table of Contents

List of Figures.....	v
List of Tables	viii
Acknowledgements.....	ix
Abstract	x
Chapter 1: Introduction	1
1.1 Overview of Batteries	1
1.2 Battery Materials	1
1.3 Battery Recycling	4
1.4 Electrodeposition	7
1.5 Thermodynamics of Phases Formation in Electrodeposition.....	8
1.5. Structure of the Thesis	11
Chapter 2: Materials and Methods	12
2.1 Materials and Equipment	12
2.2 Electrochemical Test Parameters.....	15
2.3 Characterization of Deposited Material	17
Chapter 3: Results	18
3.1 Cobalt Only Galvanostatic	18
3.2 Linear Sweep Voltammetry for Polymer Coatings	22
3.3 Deposition with Nickel and Cobalt.....	23

3.4 Deposit Material Differences	28
Chapter 4: Conclusion.....	29
References	31

List of Figures

Figure 1. The different types of battery configurations and the components, reprinted from Ref. ⁷.
(a) represents a cylindrical cell, (b) represents a prismatic cell, (c) represents a coin cell, and
(d) represents a pouch cell. In this example, LiFePO₄ is the chosen cathode material and
graphite is the anode material.3

Figure 2. Locations of cobalt mines reprinted from Ref. ⁸. The circles represent the top cobalt
producing countries, whereas the colors show the countries with the largest known reserves.
Notably the Democratic Republic of Congo contains the largest cobalt reserves, controlling
most of the cobalt sources.4

Figure 3. Battery recycling companies in 2019, reprinted from Ref. ¹². Most companies with
established recycling capabilities are either pyrometallurgical or hydrometallurgical
recycling. Direct recycling, being a relatively new process, has a few startups located in the
west United States.5

Figure 4. Schematic of the electrodeposition set-up used in this study, where counter, reference
and working electrodes are marked. Cobalt reduction reaction happens on the working
electrode. The flow of current and electrons is marked as well.8

Figure 5. Cobalt Pourbaix diagram, reprinted from Ref. ³⁷. The blue shaded region designates the
reduction region, where cobalt ions reduce to cobalt metal. The dashed line located directly
above the reduction region is the hydrogen stability line, where regions underneath it
generates hydrogen gas as a side reaction.10

Figure 6. Nickel Pourbaix Diagram, reprinted from Ref. ³⁸. The blue shaded region indicates the
reduction of nickel cations into nickel metal. (a) correlates to the hydrogen stability line and
(b) correlates to the oxygen stability line.10

Figure 7. A copper sheet used as the working electrode. Masking tape is used to cover unused regions of copper, leaving an active area for deposition where cobalt reduction occurs.13

Figure 8. Three-electrode set-up for electrodeposition in a cobalt electrolyte solution. Platinum wire is used as the counter electrode, copper sheet is the working electrode, and the reference electrode is the standard hydrogen electrode.14

Figure 9. Various polymer coatings on the working electrode. (a) consisted of the stock solution of PDADMA, creating a thick coating. (b) consisted of a 1:3 ratio of polymer to water to create a thinner coating. (c) utilized a 1:9 ratio. Notably, (b) and (c) were not able to cover the entirety of the active area..... 14

Figure 10. A linear sweep voltammetry in cobalt-only solution from 0 V to -1 V at a scan rate of 0.5 mV/s. Regions above -0.6 V were seen to not have any reactions occurring until -0.3 V, where oxidation reactions are expected. 16

Figure 11. Linear sweep voltammetry tests in cobalt-only solution from -0.4 V to -1 V. Each trial was done at a scan rate of 0.5 mV/s..... 17

Figure 12. Galvanostatic deposition tests at ranges of currents. (a) used -0.2 A, (b) used -0.25 A, and (c) used -0.3 A. (a) features deposit material that has delaminated from the active area independently and (b) features material starting to delaminate. (c) features active area that did not deposit material despite being inside the electrolyte..... 19

Figure 13. XRF tests for each galvanostatic deposit. (a) is -0.2 A, (b) is -0.25 A, and (c) is -0.3 A. Cobalt, copper, sodium, chloride, and platinum were chosen as the ions to read x-ray data for due to the presence of each in the electrodeposition setup explained in Chapter 2. Lithium oxide and carbon were machine errors measured by the XGT-9000 and were thusly disregarded.21

Figure 14. X-ray fluorescence data acquired from the XGT-9000 for the -0.3 A deposit. Cobalt is shown to have the highest intensity compared to other ions.22

Figure 15. Linear sweep voltammetry tests for the deposition of cobalt and nickel with polymer coatings on the working electrode. The addition of a coating made deposition inefficient with reduced currents and shifts in the reduction potential of cobalt.23

Figure 16. Image of both working electrodes after galvanostatic tests. (a) The electrode with polymer coating and is seen to be brighter. (b) The electrode with no coating added and is seen to be slightly darker. The deposit in (a) was found to be more of a powder texture compared to (b) and separated the working electrode easily.....24

Figure 17. Galvanostatic tests showing the change in voltage over the 5000 second duration. (a) is the polymer coating and is found to be less stable than (b), the electrode with no coating. Both are found underneath the reduction potential of cobalt, suggesting metal reduction occurs.25

Figure 18. Showcase of the points examined by x-ray fluorescence, where (a) is the polymer coated electrode and (b) is the electrode with no coating. The weight percentage of cobalt, nickel, chloride, and copper were examined at each point. The seventh point of the polymer coated electrode had a larger percentage of copper at this location.26

Figure 19. Spectrum 7 of the polymer coated electrode. The intensity of copper is the highest of all present elements, suggesting that the deposit was thin at this area, allowing x-rays to bounce from the electrode surface as well as the deposited material.28

List of Tables

Table 1. The table of the deposited mass correlated to the trial current. Increments of -0.05 A were chosen to determine how different large changes of current and deposition time affect the electrodeposit.	18
Table 2. Measured mass after galvanostatic tests for working electrodes with and without the PDADMA coating. The yield is found to be higher for the electrode with no coating.	25
Table 3. Elements observed by x-ray fluorescence. Each point was measured and an average for both working electrodes were determined. The polymer coated electrode had higher error due to the outlier point shown in Figure 16.....	26

Acknowledgements

I would like to express my appreciation for my committee chair, Professor Iryna Zenyuk, for allowing me to conduct research in her group and providing me the opportunity to delve into the topic of battery recycling. Her encouragement and support provided me with an ambition to learn more about electrochemical fundamentals and provided upliftment when I felt lost in my research. I would also like to thank Professor Diran Apelian for providing insight on current battery manufacturing and recycling for a full understanding of environmental impacts of a battery process from start to finish. And another thanks to Professor Daniel Mumm for providing me with a wealth of background knowledge of material structures and electron microscopy that made understanding x-ray data of my material straightforward.

I received helpful feedback and advice from Adrien and Bilal during my time in Dr. Zenyuk's group on various topics I presented to them before narrowing down my focus of the study. Thanks to Hung-Ming and Jesus for helping me in the lab when I was new to the space. And thanks to Cliff and Celine for helping with my XRF data.

Abstract

Electrodeposition of Cobalt and Nickel for Hydrometallurgical Lithium Ion Battery Recycling

by

Anthony Castillo Reyes

Master of Science in Engineering

University of California, Irvine, 2023

Associate Professor Iryna Zenyuk, Chair

Battery recycling is the solution for creating a closed loop system between manufacturing and production of batteries to the end-of-life batteries from cars to energy storage. With growing interest in electric vehicles creating inevitable battery waste, a scalable and efficient recycling process is needed for this increasing demand. The goal of this study is to electrochemically deposit cathode material from a leached solution to incorporate into existing hydrometallurgical battery recycling processes. Cobalt and nickel were galvanostatically deposited from a simulated leached cathode solution of NMC, producing 0.46 g of deposit material with a held current of -0.25 A for 4900 s. This material resulted in both cobalt and nickel depositing in a 1:1 ratio and is suitable for the construction of new cathode material recycling from end-of-life batteries.

Moreover, poly[diallyldimethylammonium chloride] was incorporated as an electrode coating for the separation of cobalt and nickel. This addition resulted in a lighter deposit material of 0.39 g and was found unsuccessful in separation. The inability to separate the metals was attributed to the separation occurring only at the surface of the electrode.

Chapter 1: Introduction

1.1 Overview of Batteries

Starting in the 1980s, the development of portable electronic products such as cameras and cell phones lead to the need for rechargeable batteries with restrictions in size and weight ¹. The conventional rechargeable batteries at the time were lead-acid, nickel-cadmium, and nickel-hydride batteries, all of which were still developing and had limitations due to their size and weight. This changed in 1979 when LiCoO_2 (LCO) was introduced as a cathode material by Goodenough et al. ² and further commercialized into the lithium-ion batteries consumed today by Sony in 1991 and Asahi Kasei and Toshiba in 1992 ³.

Due to the lithium-ion battery's high power density, high voltage, low weight, and low self-discharge rates, it is often used as the electrochemical power source for electronic devices. The increasing usage of electronic vehicles (EVs) and energy storage cause lithium-ion batteries (LIBs) to be popular battery technology choice due to these properties, with the production of LIBs reaching over 100 GWh in 2015 ⁴. With government regulations calling for a -50% reduction in light and medium duty-vehicle emissions in 2055 ⁵, electric vehicles are expected to further rise in popularity. Due to the growth of LIBs since its inception in 1979 and the expected continual growth, battery waste is a major concern for end-of-life batteries. From the waste, recovery of the materials by recycling is investigated for the recovery of valuable elements to ensure circular economy.

1.2 Battery Materials

A battery consists of three major components that are the cathode, anode, and electrolyte, where two redox half-reactions occur to create the full electrochemical reaction of the battery. The cathode material consists of active material, binder, and current collector. The active

material includes various compositions of transition metal oxides with lithium ($\text{LiNi}_{1-x-y}\text{Mn}_x\text{Co}_y\text{O}_2$, LiFePO_4 , LiCoO_2 , LiMn_2O_4)⁶. The anode material is commonly a graphite material, current collector, and a binder where lithium ions are intercalated during the charging cycle of a battery. The current collectors consist of copper for the anode side and aluminum for the cathode side. The binders for both materials consist of polyvinylidene fluoride (PVDF). The electrolyte consists of a lithium salt dissolved in an organic solvent, where the salt is LiPF_6 and the solvent is a carbonate. This electrolyte is soaked into a microporous film of polymer, known as a separator, that electrically insulates anode and cathode and enables ion conduction between the two electrodes. Figure 1 showcases the different types of battery configurations and each component⁷.

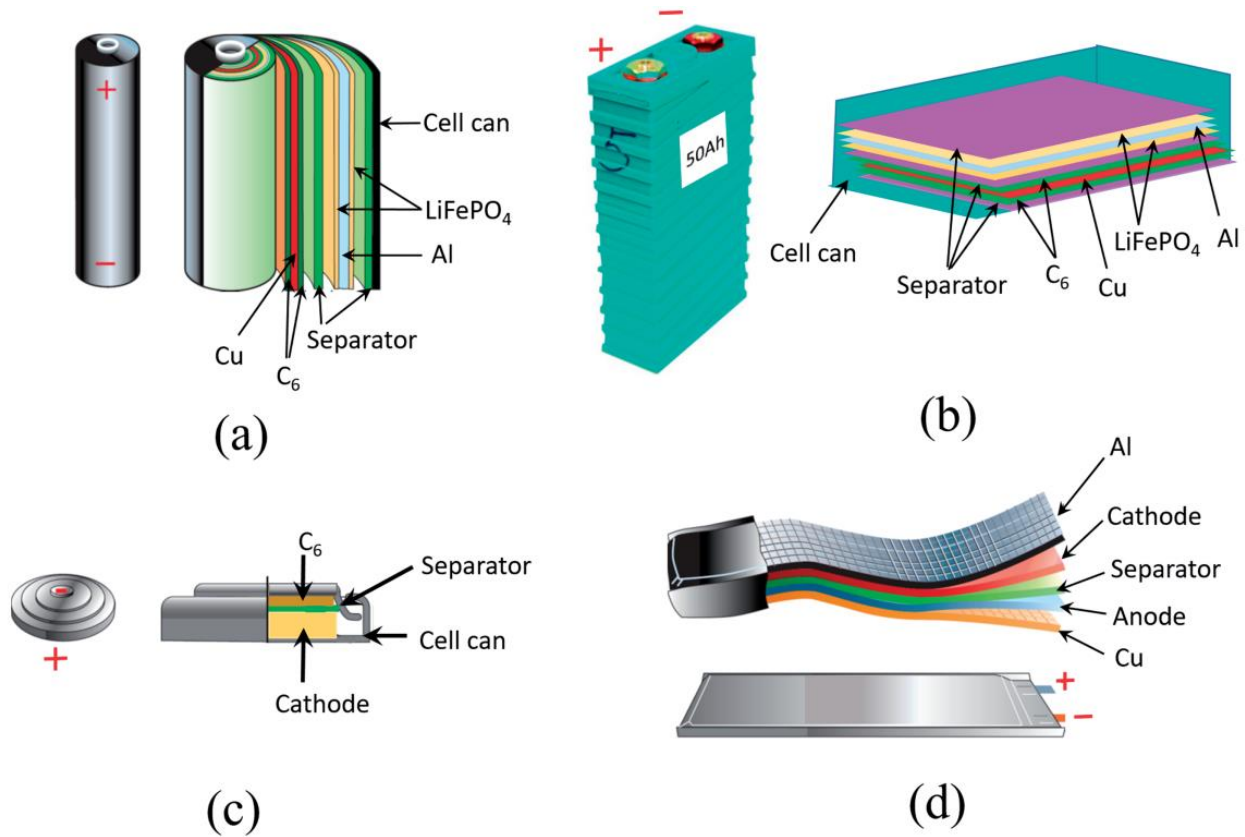


Figure 1. The different types of battery configurations and the components, reprinted from Ref. ⁷. (a) represents a cylindrical cell, (b) represents a prismatic cell, (c) represents a coin cell, and (d) represents a pouch cell. In this example, LiFePO₄ is the chosen cathode material and graphite is the anode material.

The material that is of interest is the cathode material due to the critical earth elements present in the material, namely the cobalt. Figure 2 showcases the locations of cobalt mines around the world, where the Democratic Republic of Congo (DRC) contains the most reserves, making cobalt a commodity monopolized by the DRC ⁸. The presence of unregulated artisanal mining in the DRC creates unsafe work conditions and child labor, making the social issues prevalent ⁹. Despite negative connotations regarding the DRC mining, cobalt obtained from the DRC is still used in current battery technology, supplying 73% of the 198 kilotons mined in 2022 ¹⁰. The refining of cobalt is also monopolized as China has close relations with the DRC. Chinese refineries are estimated to make up 46% of the refined cobalt supply, with companies such as Quzhou Huayou having direct links between their mines in the DRC and their refineries in China ¹¹. Cobalt's supply is vital as 40% of the cobalt share is in the EV sector and 30% in portables ¹⁰. This study aims to investigate the recycling of cobalt from the cathode material due to the projected growth of battery technology, and to circumvent the monopolization of cobalt supply.

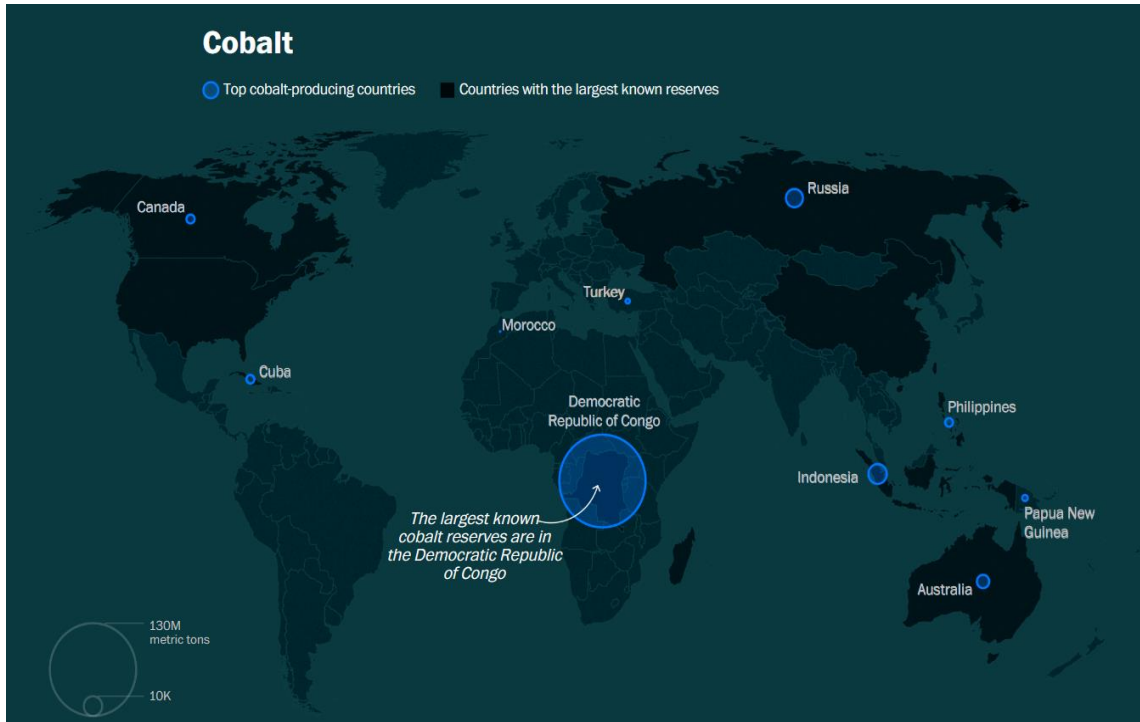


Figure 2. Locations of cobalt mines reprinted from Ref.⁸. The circles represent the top cobalt producing countries, whereas the colors show the countries with the largest known reserves. Notably the Democratic Republic of Congo contains the largest cobalt reserves, controlling most of the cobalt sources.

1.3 Battery Recycling

Methods for recycling battery components consist of three different technologies: pyrometallurgical, hydrometallurgical, and direct recycling¹². Pyrometallurgical recycling utilizes high temperature furnaces with a slag-forming agent to smelt battery components into a mixed alloy, consisting of cobalt, copper, iron, and nickel¹³. This method recovers only expensive metals from the battery cathode and current collectors. Furthermore, pyrometallurgical recycling methods emit fluorinated gas from the oxidation of the PVDF binder that are an environmental concern¹⁴. Hydrometallurgical recycling first starts with a separation process of dismantling and separating the battery into its individual components, then the materials are

leached in acid and ions in the solution are recovered ¹⁵. This method recovers most battery components due to the separation process and each element is either separated ¹⁶ or reconstituted into new battery cathode material ¹⁷. Direct recycling also starts with a similar separation process, but instead consists of a re-lithiation process where new lithium is added to the spent cathode material ¹⁸. This method maintains the structure of the previous spent battery but requires further separation than hydrometallurgical processes. As both pyrometallurgical and hydrometallurgical are shown to be commercially ready compared to direct recycling as seen in Figure 3, direct recycling was not investigated ¹². And due to the high energy consumption of pyrometallurgical processes from the high temperature required creating upwards of 2350 kg CO₂-eq. per ton of LIB ¹⁹, hydrometallurgical recycling was the chosen method investigated in this study.

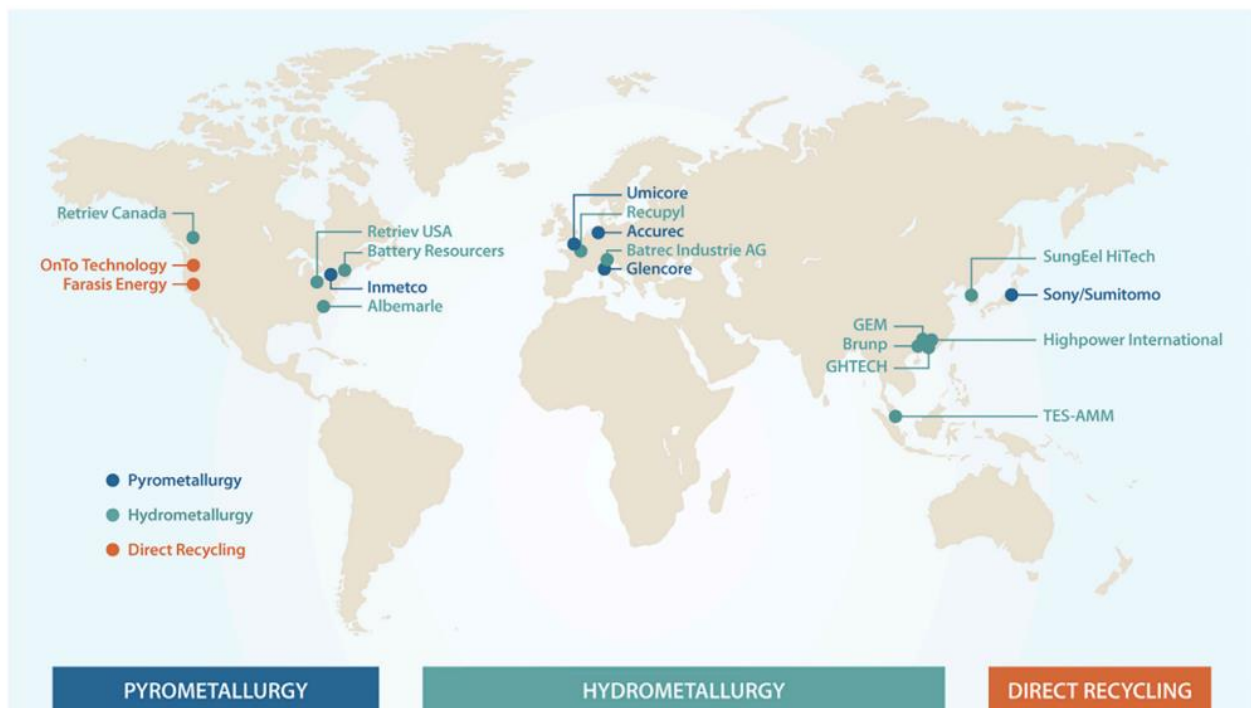


Figure 3. Battery recycling companies in 2019, reprinted from Ref.¹². Most companies with established recycling capabilities are either pyrometallurgical or hydrometallurgical recycling.

Direct recycling, being a relatively new process, has a few startups located in the west United States.

In hydrometallurgical recycling, there are two general methods of separating the elements in the leached solution: non-electrochemical and electrochemical recovery^{20,21}. For non-electrochemical recovery, there are various ways to recover elements by either separating each element or reconstituting the end product into various alloys and cathode materials, with both methods utilizing additional chemicals for recovery. Solvent extraction is a method that uses solvents such as D2EHPA (di-(2-ethylhexyl) phosphoric acid) to extract ions by utilizing the different solubilities of the metal ion²². Notably, solvent extraction uses hazardous chemicals for separation due to the insolubility in water properties needed for separation²³. Chemical precipitation is another method of recovery that utilizes precipitants, such as H₃PO₄, and pH control to precipitate out the metal ions²⁴. Notably, chemical precipitation can either selectively precipitate elements²⁵ or directly precipitate as a precursor hydroxide and subsequently oxidize into cathode material²⁶.

For electrochemical recovery, the various methods for recovery of metals include electrodeposition, electrosorption, electro dialysis, and electrocoagulation²⁰. Electrodeposition utilizes an applied current to the leached solution through two electrodes to deposit metal by a reduction reaction, and the deposition of cobalt has been widely investigated^{27,28}. Although electrodeposition has difficulty incorporating selectivity, Kim et al. has successfully separated cobalt and nickel by usage of a polymer coating²⁹. Electrosorption, known as electrical field-assisted adsorption, uses a potential difference to migrate charged ions towards a polarized electrode and separate the ions from the liquid phase³⁰. Cobalt has been removed by this method, utilizing capacitive deionization, but results in a low removal efficiency of 36.5%³¹.

Electrodialysis uses both an ion exchange membrane and an electrochemical potential to separate ions, and the separation of cobalt and nickel has successfully been investigated by Sadyrbaeva with the addition of a liquid membrane³². Electrocoagulation uses a sacrificial anode to split water into hydrogen and hydrogen ions, consequently hydrolyzing metal cations, binding to other ions and particles, thus creating a coagulant³³. Shafaei et al. reported successful cobalt recovery from their prepared solutions using aluminum electrodes as a sacrificial anode³⁴.

From these options, electrodeposition was chosen with this study. Solvent extraction utilized expensive materials that required further solvent recovery steps²² and chemical precipitation utilized additional chemicals, such as oxalic acid, to selectively precipitate ions³⁵. An initial test was done using solvent extraction methods utilizing an ionic liquid (C₄mim NTf₂) but was not chosen due to high cost³⁶. Electrosorption and electrocoagulation were not chosen due to studies utilizing these methods for wastewater recovery without the presence of nickel, a common element for NMC lithium-ion batteries. Electrodialysis featured liquid membranes for ion exchange but were high in cost and not suitable for scaling. Electrodeposition studies for cathode material separation utilize salts already present in the leached solution (LiCl) as electrolyte for the background electrolyte³⁷.

1.4 Electrodeposition

Electrodeposition is a process of reduction of metal cations onto a plate by a direct current. As shown in Figure 4, electrodeposition utilizes a three-electrode system in electrolyte, where the three electrodes consist of the working electrode, counter electrode, and reference electrode. The working electrode is the electrode where reduction of the metal ion occurs. The counter electrode allows current to pass through the system and is an inert metal so as to not participate in reaction. The reference electrode is used to measure the potential of the working

electrode. The electrolyte contains metal cations for deposition as well as consisting of additional salts to transport ions in the system.

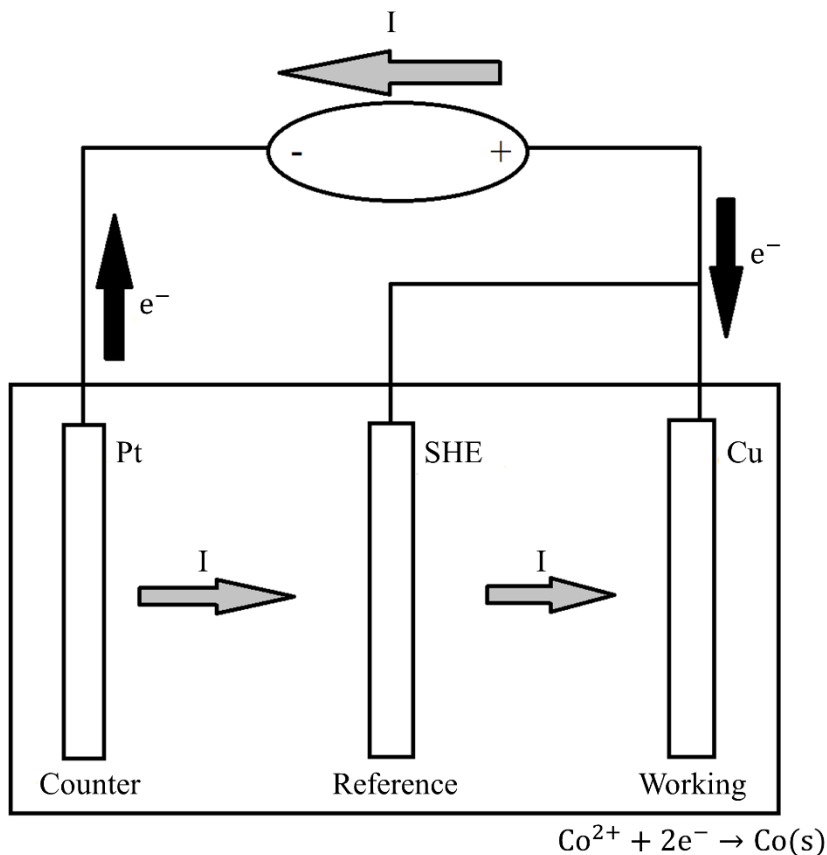


Figure 4. Schematic of the electrodeposition set-up used in this study, where counter, reference and working electrodes are marked. Cobalt reduction reaction happens on the working electrode. The flow of current and electrons is marked as well.

1.5 Thermodynamics of Phases Formation in Electrodeposition

Pourbaix diagrams are plots of potential vs. pH where the lines indicate a phase the material is in. To determine the needed voltage applied and pH of the electrolyte, the Pourbaix diagram shown in Figure 5 was used³⁷. As cobalt reduction is the reaction of interest from Co^{2+} to Co, the cobalt metal region was used, where a voltage of -0.45 V or lower and a pH of 9 or

lower were needed for reduction to occur, as shown in the blue shaded region in Figure 5. As this region is underneath the hydrogen stability line, labeled by its chemical reaction in Figure 5, hydrogen evolution is expected to occur as a side reaction alongside cobalt reduction. The Pourbaix diagram for nickel was also investigated in Figure 6³⁸. Both reduction potentials of nickel and cobalt are found to be under the hydrogen stability line, so hydrogen gas evolution is expected as a side reaction. Nickel and cobalt are also found to reduce into metal at similar potentials and pH, causing the deposition of both elements to occur simultaneously. Due to the similarity, a polymer coating was utilized to facilitate the separation in the electrodeposition recovery, discussed in Chapter 2.1.

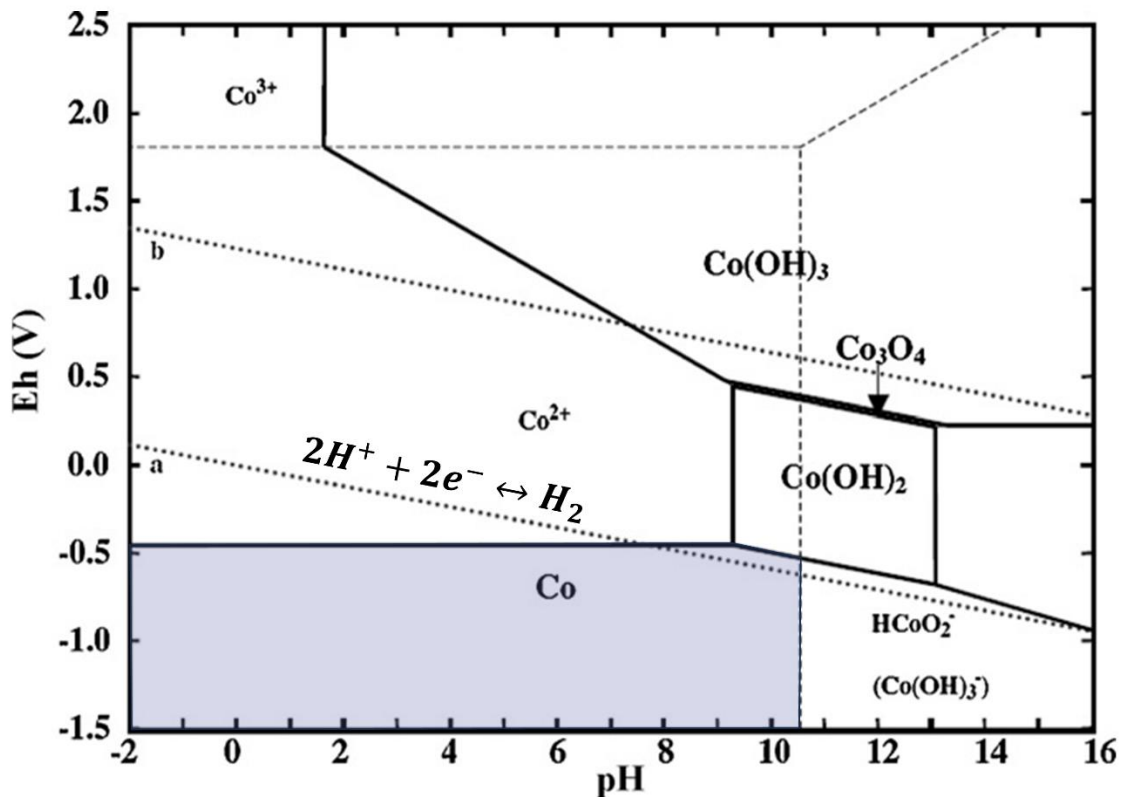


Figure 5. Cobalt Pourbaix diagram, reprinted from Ref.³⁷. The blue shaded region designates the reduction region, where cobalt ions reduce to cobalt metal. The dashed line located directly above the reduction region is the hydrogen stability line, where regions underneath it generates hydrogen gas as a side reaction.

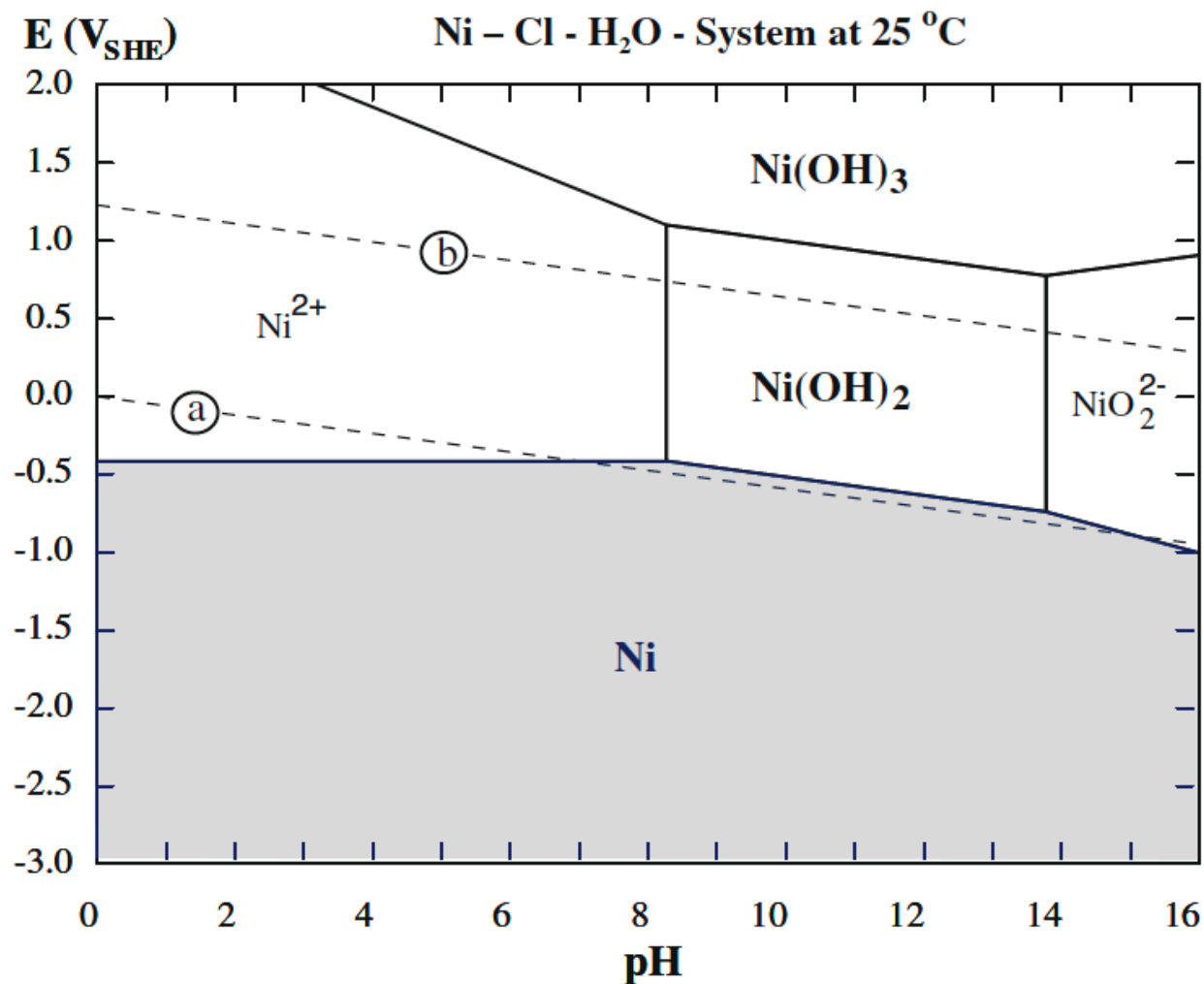


Figure 6. Nickel Pourbaix Diagram, reprinted from Ref.³⁸. The blue shaded region indicates the reduction of nickel cations into nickel metal. (a) correlates to the hydrogen stability line and (b) correlates to the oxygen stability line.

To determine the efficiency of the deposition, Faraday's Law was utilized ³⁹:

$$m = \frac{M \times I \times t}{\frac{n}{s} \times F}. \quad (1)$$

The mass 'm' was determined theoretically and compared to the measured mass of the system once deposition occurred. 'M' is the molar mass of the desired cobalt deposit. 'I' is the current applied to the system. 't' is the length of time the system was applied current. 'n' is the number of electrons involved in the reaction, equaling 2. 's' is the stoichiometric coefficient of cobalt, equaling 1. 'F' is the Faraday's constant, $96,485 \frac{C}{mol}$.

1.5. Structure of the Thesis

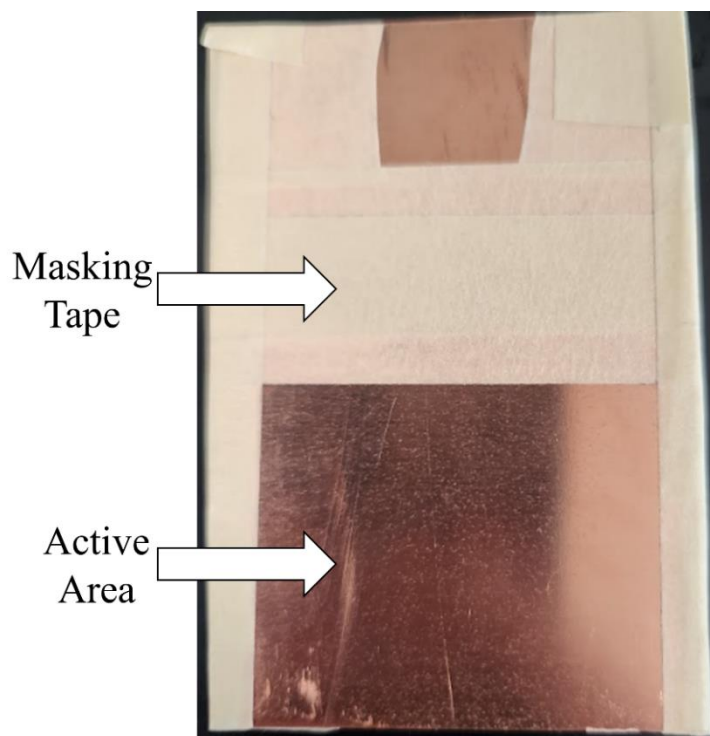
The main goal of the thesis is to introduce electrochemical recovery in the hydrometallurgical process and determine the efficiency of this recovery method. The novelty of the work is testing electrodeposition by galvanostatic to emulate manufacturing conditions, as opposed to linear sweep voltammetry ²⁹. In Chapter 2 I will introduce the methods utilized in preparing the electrodeposition test as well as the characterization of the deposit. In Chapter 3 I will show the experimental results of tests done with only cobalt ions, and tests done separating nickel and cobalt. Lastly, Chapter 4 will provide conclusions and future work recommendations.

Chapter 2: Materials and Methods

2.1 Materials and Equipment

In this study, two solutions were created for the deposition of cobalt material. The solutions consisted of cobalt (II) chloride hexahydrate (Sigma-Aldrich, $\geq 97\%$), nickel (II) chloride (Sigma-Aldrich, 98%), and sodium chloride (Sigma-Aldrich, $>99\%$). The first solution consisted of 0.1 mol/L of CoCl_2 and 2.00 mol/L of NaCl in a 200 mL solution, diluted by deionized water. The second solution consisted of similar molarities in deionized water, with the addition of 0.1 mol/L of NiCl_2 . The solutions were mixed and placed in a 1000 mL beaker (Amazon, Fisher Scientific). These solutions were used as the electrolyte for three-electrode set-up for electrodeposition. Notably, the concentration of chloride ions was important for cobalt due to the formation of an anionic complex, CoCl_4^{2-} ⁴⁰. This complex has been documented to be critical for an underlying mechanism for the separation of nickel and cobalt^{32,41}.

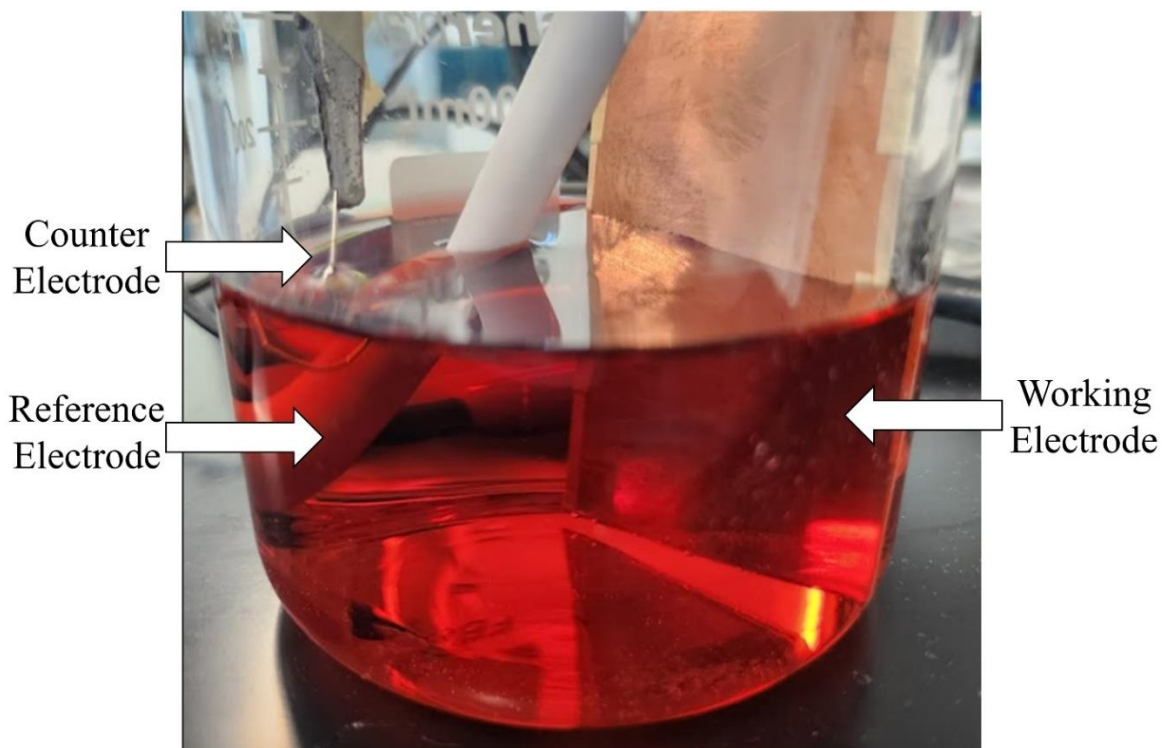
The electrode set-up consisted of a working electrode, reference electrode, and counter electrode. Platinum wire (Sigma-Aldrich, 0.25 mm diameter, 99.9%) was used as the working electrode. The reference electrode was a Hydro Flex hydrogen reference electrode (Gakatel). The counter electrode was a copper sheet obtained from McMaster-Carr (2" x 36", 0.0200" thickness). The platinum wire was cut into a length of 7 cm and coiled into a spiral. The copper sheet was cut into a 7 cm x 5 cm piece to fit into the beaker of electrolyte. To ensure only a set region of the counter electrode was exposed to the deposition, masking tape (Amazon, Scotch) was used to cover undesired regions, leaving an active area of 4 cm x 5 cm, as shown in Figure 7. An example of the three-electrode set-up is shown in Figure 8.



Masking
Tape

Active
Area

Figure 7. A copper sheet used as the working electrode. Masking tape is used to cover unused regions of copper, leaving an active area for deposition where cobalt reduction occurs.



Counter
Electrode

Reference
Electrode

Working
Electrode

Figure 8. Three-electrode set-up for electrodeposition in a cobalt electrolyte solution. Platinum wire is used as the counter electrode, copper sheet is the working electrode, and the reference electrode is the standard hydrogen electrode.

A polymer coating was added onto the working electrode afterwards for the selectivity of nickel deposition due to the polymer inhibiting cobalt. The polymer utilized was poly[diallyldimethylammonium chloride] solution (Sigma-Aldrich, 200,000-350,000 average molecular weight), labeled forward as PDADMA. The polymer works in separating nickel from cobalt due to the amine group reacting with the cobalt complex formed ⁴². This coating was first tested directly onto the working electrode with no additions, labeled forward as the stock solution and shown in Figure 9a. The coating was then diluted in various ratios of deionized water to create a thinner coating. The coatings tested are found in Figure 9.

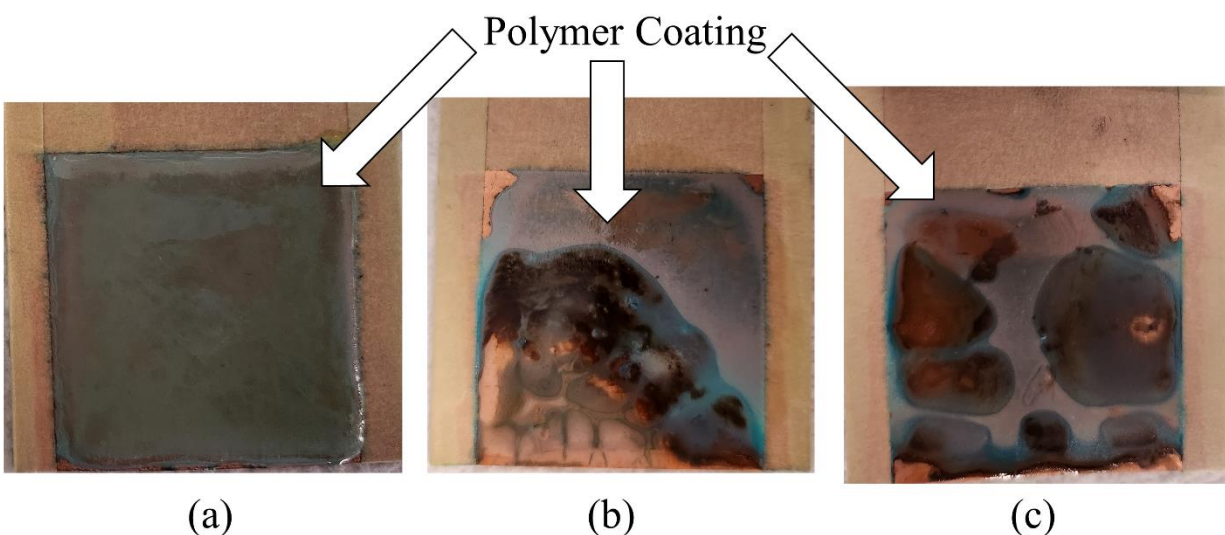


Figure 9. Various polymer coatings on the working electrode. (a) consisted of the stock solution of PDADMA, creating a thick coating. (b) consisted of a 1:3 ratio of polymer to water to create a thinner coating. (c) utilized a 1:9 ratio. Notably, (b) and (c) were not able to cover the entirety of the active area.

The instrument utilized for the electrodeposition was the Gamry Interface 1010 (Gamry). Two types of tests were conducted using the Gamry Interface: linear sweep voltammetry (LSV) and chronopotentiometry. The LSV determined the regions in which the deposition reactions occurred and the chronopotentiometry was used to maintain consistent current and voltage for the depositing of material.

2.2 Electrochemical Test Parameters

To determine the parameters of current and voltage in which future LSV and chronoamperometry tests would be performed with, a preliminary LSV was done. This sweep utilized the cobalt-only electrolyte solution for determining the parameters for the reduction of cobalt ions to cobalt metal. Figure 10 showcases this preliminary LSV. From the data, the cobalt reduction reaction occurs after -0.6 V.

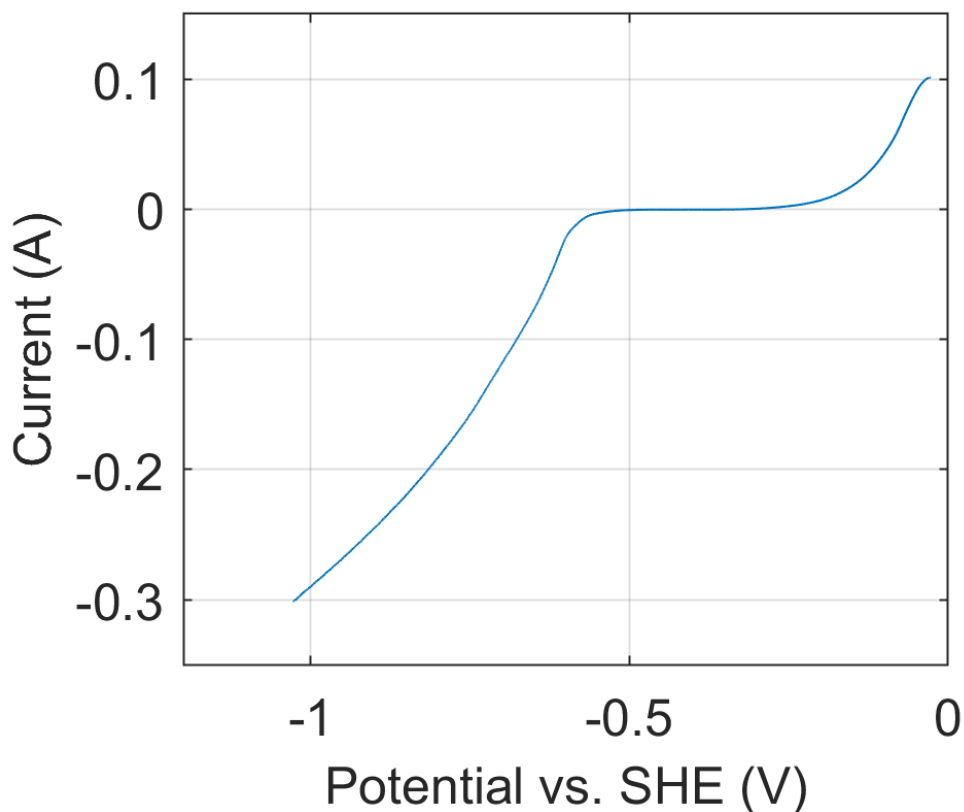


Figure 10. A linear sweep voltammetry in cobalt-only solution from 0 V to -1 V at a scan rate of 0.5 mV/s. Regions above -0.6 V were seen to not have any reactions occurring until -0.3 V, where oxidation reactions are expected.

Further testing in the reduction region of cobalt was done to accurately determine the current and voltage to conduct chronoamperometry tests. Figure 11 shows the currents in which the reduction occurs. From this test, -0.2 A was found to correlate to a voltage of -0.9 V with a linear relationship between current and voltage. Tests ranging from -0.2 A and below were used for chronoamperometry tests due to the direct relationship between the current used and the time to deposit material explained by Faraday's Law. In the interest in having a faster reaction for better scalability, a higher amperage was chosen.

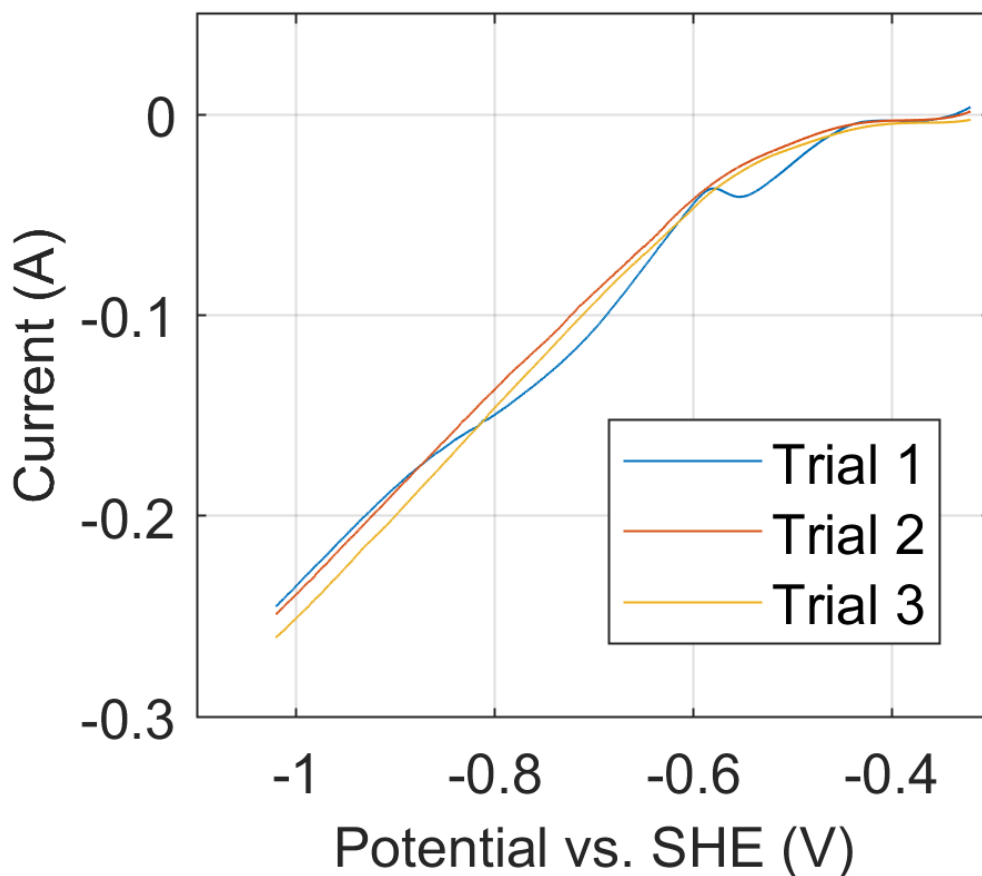


Figure 11. Linear sweep voltammetry tests in cobalt-only solution from -0.4 V to -1 V. Each trial was done at a scan rate of 0.5 mV/s.

2.3 Characterization of Deposited Material

The instrument utilized for characterization of the deposited material was the XGT-9000 (Horiba). This instrument utilizes an incident X-ray beam on the sample to obtain X-ray fluorescence spectrum and transmission intensity data to determine the composition of the deposited material. The instrument features a program that determines the energy released from the characteristic X-rays emitted by the elements in the deposited material. This was checked with the $K\alpha$ emissions calculated by Moseley's Law ⁴³:

$$E = R \times \left(\frac{1}{n_f^2} - \frac{1}{n_i^2} \right) (Z - 1)^2 \quad (2)$$

'E' represents the expected energy emission from the characteristic X-rays. 'R' is Rydberg's constant, equivalent to approximately 13.6 eV. 'n_f' and 'n_i' are the final and initial quantum levels, which are 1 and 2 respectively for $K\alpha$ emissions. 'Z' is the atomic number of the element. Cobalt's $K\alpha$ emission is 6.90 keV and nickel is 7.44 keV, both found using Moseley's Law and will be compared to the XRF results found in Chapter 3. From the intensity peaks, the fundamental parameters method was utilized to quantify the elements present in the deposit material ^{44,45}.

Chapter 3: Results

3.1 Cobalt Only Galvanostatic

After the LSV tests described in Chapter 2, currents below -0.2 A were determined to be ideal for testing deposition with a fast rate. Tests were done by using a specified current in the chronopotentiometry scan test mode for the Gamry Interface 1010. To ensure the galvanostatic tests yielded the same theoretical yield, a consistent 0.373 g was decided as the desired mass. From this, Faraday's Law was used to determine the time needed for set currents as shown in Table 1, where increments of -0.05 A were chosen for the trials to test differences of large current changes. The table also features the mass of the deposit, measured physically by a weight scale after electrochemical tests, where the trial of -0.25 A was determined to be the closest to the desired mass. Yield increased as the current decreased and time increased, equating to current being used by side reactions for -0.25 A and -0.3 A such as chlorine gas evolution observed by its residual scent or hydrogen evolution expected from the Pourbaix diagrams in Chapter 1.5. A higher yield of 121% for -0.2 A was observed, linked to the delamination found in the deposit material. This delamination created a larger surface area than anticipated, allowing for more reactions to occur. Figure 12 shows the deposit material and copper working electrode for the -0.2 A, -0.25 A, and -0.3 A trials, where the -0.2 A trial featured delamination. The -0.25 A trial was shown to produce the most uniform deposit. Notably copper active area can be seen in both the -0.2 A and -0.3 A tests.

Table 1. The table of the deposited mass correlated to the trial current. Increments of -0.05 A were chosen to determine how different large changes of current and deposition time affect the electrodeposit.

Trial Current (A)	Normalized Current (A/cm ²)	Time (s)	Deposit Mass (g)	Yield
-0.2	-0.8	6098	0.45	121%
-0.25	-0.01	4879	0.33	88.7%
-0.3	-0.012	4066	0.30	80.2%

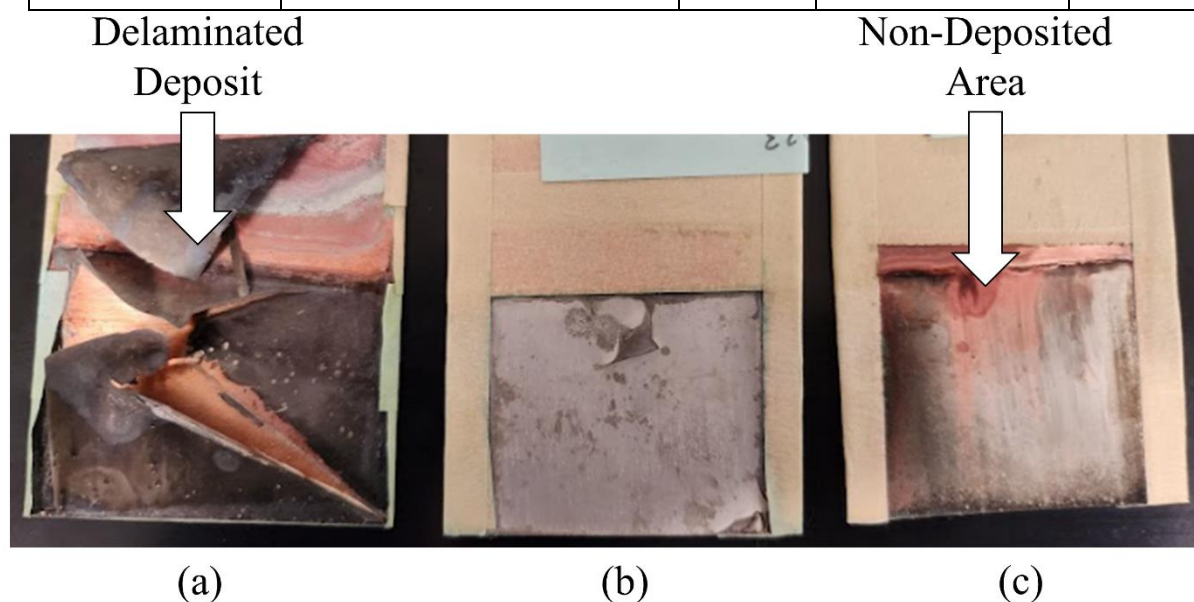


Figure 12. Galvanostatic deposition tests at ranges of currents. (a) used -0.2 A, (b) used -0.25 A, and (c) used -0.3 A. (a) features deposit material that has delaminated from the active area independently and (b) features material starting to delaminate. (c) features active area that did not deposit material despite being inside the electrolyte.

After the deposition tests, the material was then characterized using XRF to determine purity of the cobalt samples. Figure 13 shows each material that was analyzed and the concentration of the ions present. Each element was chosen due to the presence of each from the experimental setup. From the tables, cobalt has the highest concentration, as expected. Differing between each deposit, however, is the concentration of cobalt between each as the elements present in the experimental setup are analyzed. The chloride ions present in each sample are due

to the dried out electrolyte, where the salt ions are still present. Copper ions appeared due to x-rays passing through the deposit material and being absorbed by the copper electrode surface. This is present in the -0.3 A deposit, where the deposit material is thinner, and minimal in the -0.2 A deposit, where the deposit material peeled from the surface. Sodium and platinum ions were at low intensities compared to cobalt and were deemed negligible. Light elements such as lithium oxide and carbon are unable to be detected by hard x-rays due to predominate emissions of Auger electrons compared to characteristic x-rays after excitation⁴⁶, so the measurements of these are considered artifacts of the XGT-9000 system and disregarded. Figure 14 shows the intensities of each element, where cobalt is seen as the highest, while other elements such as platinum and sodium do not have prominent intensity peaks. The -0.25 A deposit is found to be the highest purity of cobalt as each other ion is found in concentrations less than 1% as opposed to the other deposited material as was chosen as the ideal current moving forward.

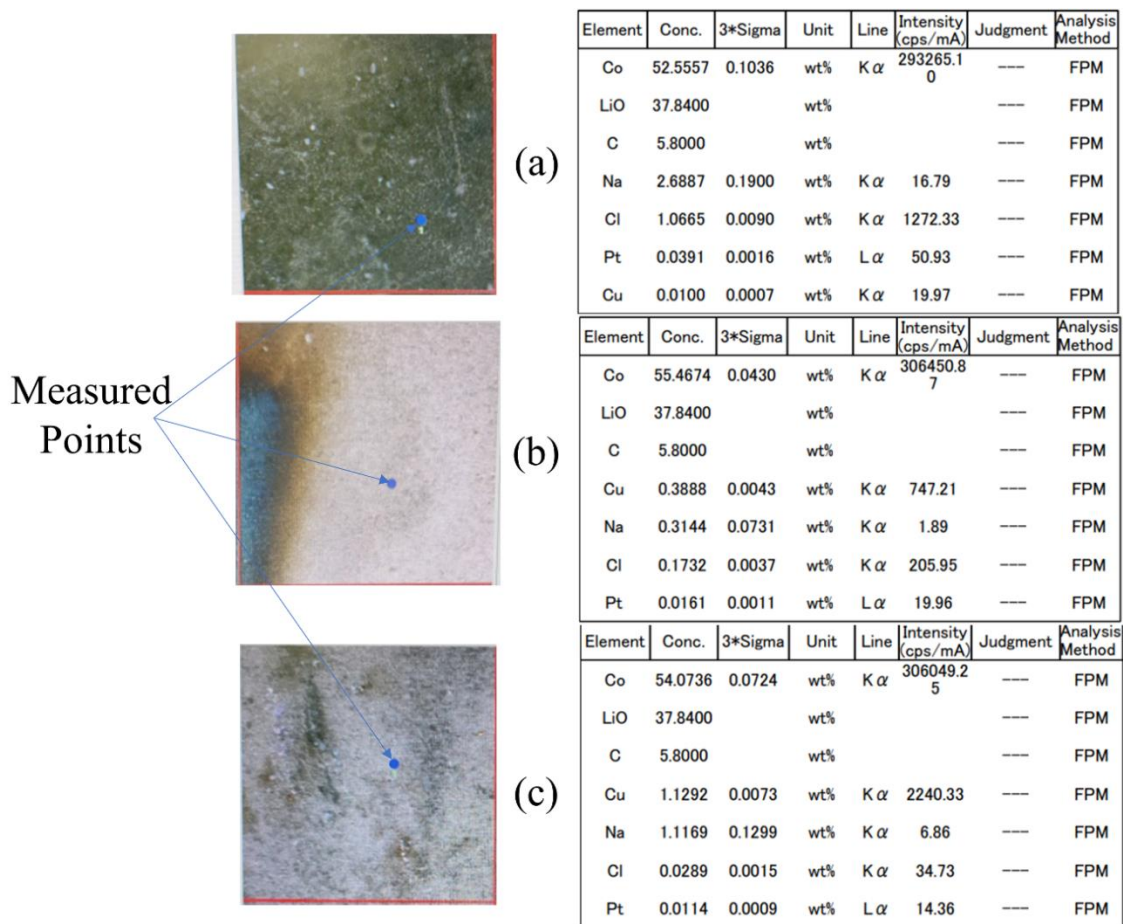


Figure 13. XRF tests for each galvanostatic deposit. (a) is -0.2 A, (b) is -0.25 A, and (c) is -0.3 A. Cobalt, copper, sodium, chloride, and platinum were chosen as the ions to read x-ray data for due to the presence of each in the electrodeposition setup explained in Chapter 2. Lithium oxide and carbon were machine errors measured by the XGT-9000 and were thusly disregarded.

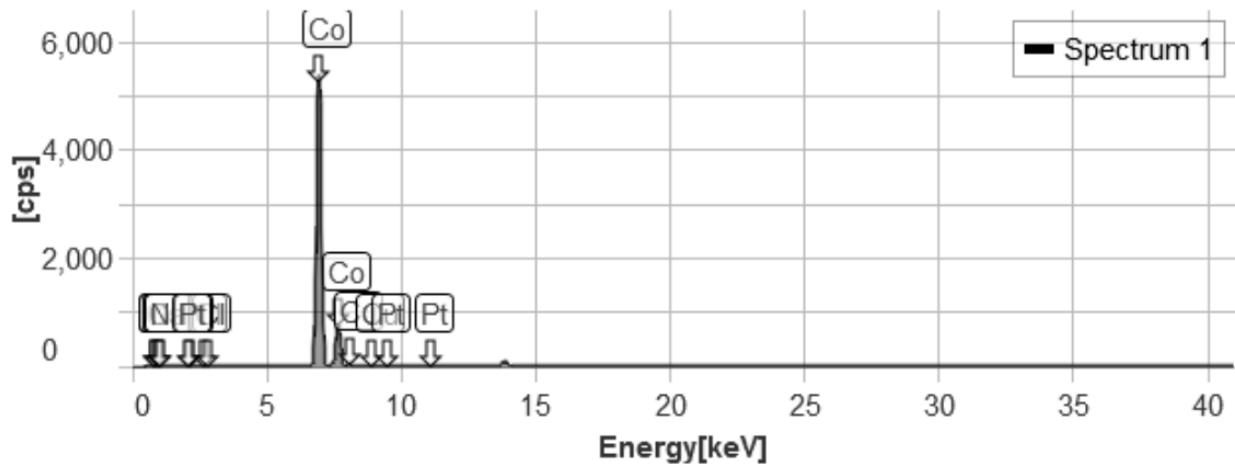


Figure 14. X-ray fluorescence data acquired from the XGT-9000 for the -0.3 A deposit. Cobalt is shown to have the highest intensity compared to other ions.

3.2 Linear Sweep Voltammetry for Polymer Coatings

To determine the polymer coating best suited for testing the deposition of cobalt and nickel, LSV tests were performed for the varying amounts of polymer diluted by deionized water. These tests were done with the polymer solution without change from the supplier, a ratio of 1 part polymer solution to 3 parts deionized water, and a ratio of 1 to 9. The results of the LSV tests are shown in Figure 15. The polymer stock solution was found to have a negative shift of 0.2 V in where the deposition reaction occurs, while the diluted polymer solutions also shifted, but to a smaller degree of 0.05 V. There is also a reduction in current for all coatings compared to the test with no coating, indicating a lower reaction rate for deposition. From this test, the most diluted polymer solution was chosen to compare to no coating for the deposition of cobalt and nickel to determine how effective PDADMA is a selectively separating cobalt ²⁹.

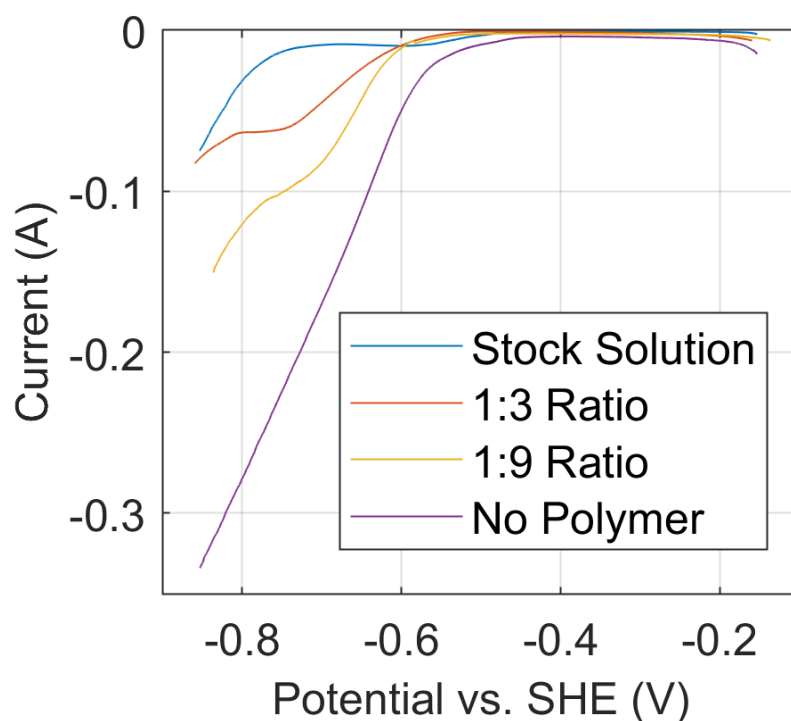


Figure 15. Linear sweep voltammetry tests for the deposition of cobalt and nickel with polymer coatings on the working electrode. The addition of a coating made deposition inefficient with reduced currents and shifts in the reduction potential of cobalt.

3.3 Deposition with Nickel and Cobalt

After determining the polymer coating to test and compare to the non-coated electrode, the same galvanostatic test done in Chapter 3.1 was performed, where -0.25 A was held for 4900 seconds. Figure 16 shows the deposited material, where there is a difference in color, likely due to the different element ratio of the deposit. The deposited material on the polymer coated electrode was also found to have a powder texture that separated from the electrode surface easily. Table 2 further shows the difference between the two material, where the electrode with no coating is found to have a higher yield than the polymer coated electrode as expected. The expected material deposited was found again utilizing Faraday's Law, but assumed half of the

current went towards the reduction of cobalt and the other half went towards nickel reduction. This resulted in a theoretical deposit weight of 0.373g, similar to the cobalt only deposited material. Both tests resulted in a higher yield than the theoretical amount. This is due to assumptions of how many electrons were present in the reaction being constant, both nickel and cobalt were nickel (II) and cobalt (II) ions, and assuming only cobalt and nickel reduction reactions occurring. Figure 17 shows how stable the voltage was during the galvanostatic test, where the non-coated electrode held stable after 300 seconds while the polymer coated electrode varied greater. This is due to fluctuations in the resistance of the material, which is discussed in 3.4.

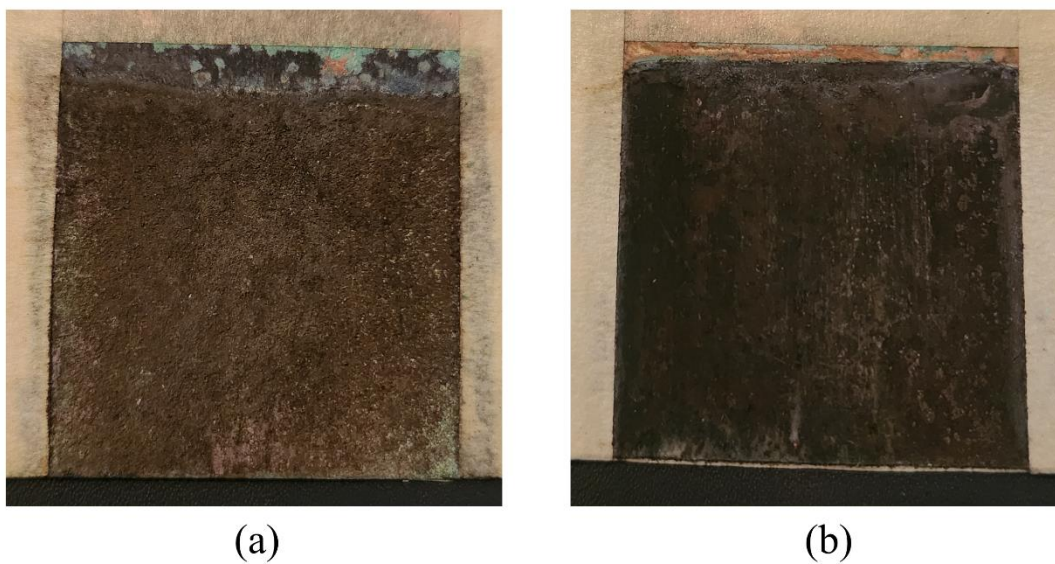


Figure 16. Image of both working electrodes after galvanostatic tests. (a) The electrode with polymer coating and is seen to be brighter. (b) The electrode with no coating added and is seen to be slightly darker. The deposit in (a) was found to be more of a powder texture compared to (b) and separated the working electrode easily.

Table 2. Measured mass after galvanostatic tests for working electrodes with and without the PDADMA coating. The yield is found to be higher for the electrode with no coating.

Coating	Deposit Mass (g)	Yield
No Coating	0.46	124%
Polymer Coating	0.39	105%

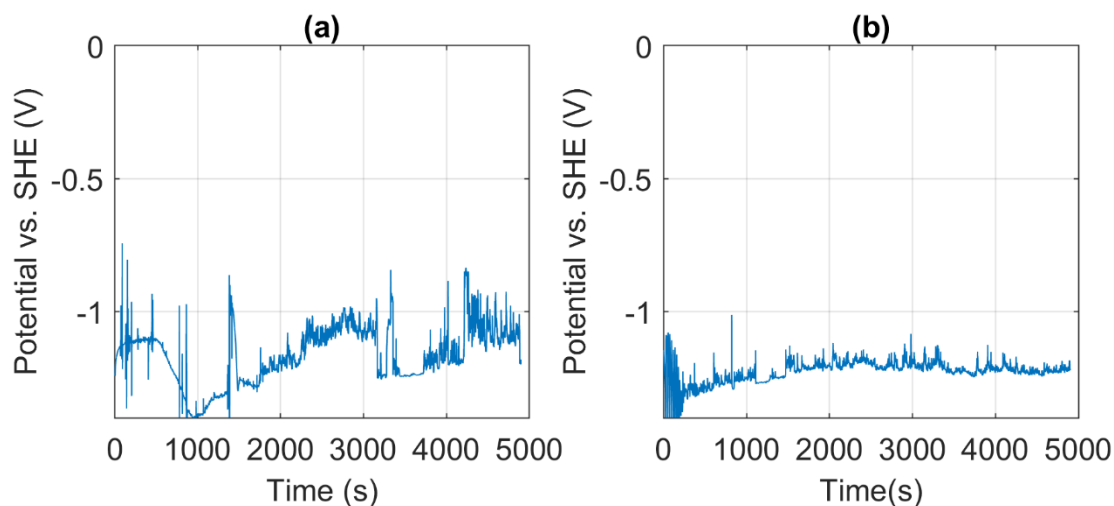


Figure 17. Galvanostatic tests showing the change in voltage over the 5000 second duration. (a) is the polymer coating and is found to be less stable than (b), the electrode with no coating. Both are found underneath the reduction potential of cobalt, suggesting metal reduction occurs.

To characterize the deposit, XRF was done on both deposited material to determine the element ratios of each. Figure 18 shows the points chosen to determine the ratio of elements of the deposit. Nine different points were chosen at regular intervals and the ratios of cobalt, nickel, chlorine, and copper were found. Table 3 shows the average ratio of each element with its standard deviation and error. Firstly, the concentration of cobalt and nickel are noticeably similar for the deposit with coating compared to the one without, with both having almost a one to one ratio of cobalt to nickel. Second, copper is a noticeable element in the polymer coating deposit at

11% while for the non-coated material, it is only 2%. This is due to the outlier of spectrum 7 in the polymer coating, highlighted in Figure 18. Lastly, chloride is consistent between both deposits, coming from salt deposition during drying of the electrolyte. The chloride results in 0.01 grams of the deposit material for both tests. Looking closer at the results shown in Figure 19, we can see that copper is at the highest intensity, suggesting that the deposit did not deposit uniformly, exposing the working electrode surface.

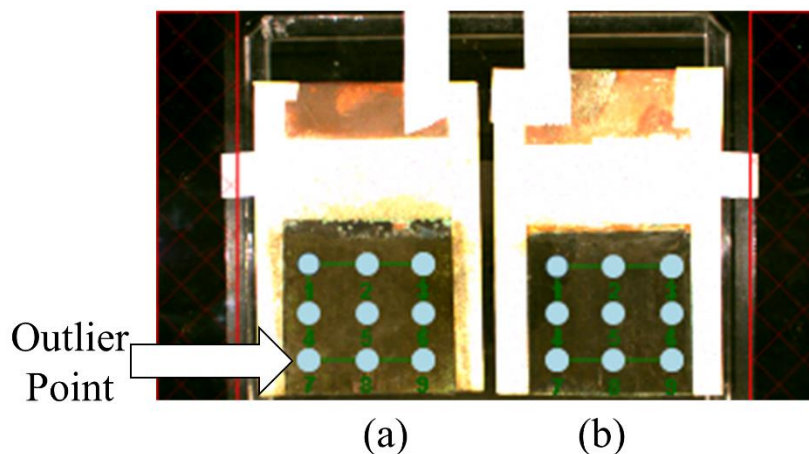


Figure 18. Showcase of the points examined by x-ray fluorescence, where (a) is the polymer coated electrode and (b) is the electrode with no coating. The weight percentage of cobalt, nickel, chloride, and copper were examined at each point. The seventh point of the polymer coated electrode had a larger percentage of copper at this location.

Table 3. Elements observed by x-ray fluorescence. Each point was measured and an average for both working electrodes were determined. The polymer coated electrode had higher error due to the outlier point shown in Figure 16.

No Coating			
Element	Concentration (wt%)	Error	Standard Deviation
Cobalt	47.8	0.224	0.673
Nickel	48.2	0.331	0.992
Chloride	1.98	0.258	0.775
Copper	2.01	0.255	0.764
Polymer Coating			
Element	Concentration (wt%)	Error	Standard Deviation
Cobalt	42.7	2.52	7.55
Nickel	43.0	2.58	7.74
Chloride	3.05	0.307	0.921
Copper	11.3	5.00	15.0

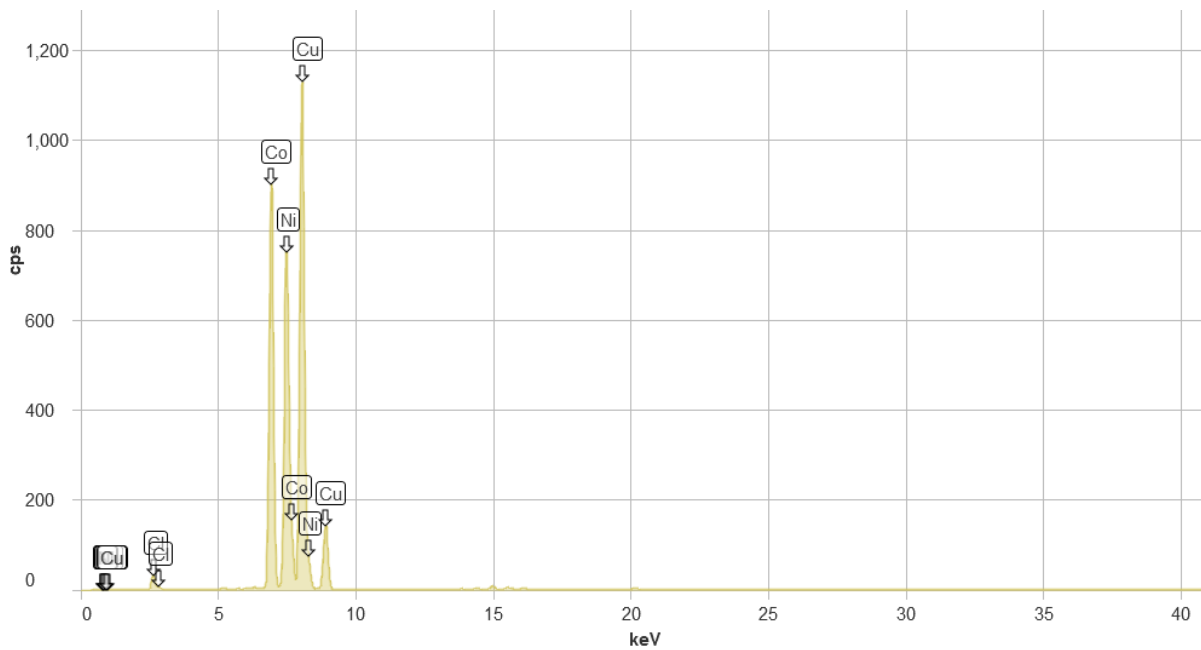


Figure 19. Spectrum 7 of the polymer coated electrode. The intensity of copper is the highest of all present elements, suggesting that the deposit was thin at this area, allowing x-rays to bounce from the electrode surface as well as the deposited material.

3.4 Deposit Material Differences

From the element composition determined by x-ray fluorescence in Table 3, the PDADMA polymer coating was ineffective from separating cobalt and nickel in electrodeposition despite a previous study showing otherwise²⁹. This is likely due to the scale difference between the tests done, where tests done by Kim et al. occurred for 600 seconds and deposited 0.00004 grams while tests done in this thesis were done for 4900 seconds and deposited 0.373 grams. The polymer inhibiting cobalt deposition occurs only at the surface of the electrode and once material is deposited, the inhibition effect decreases until cobalt and nickel are reduced simultaneously. The mass measured in Table 2 also suggests that the polymer coated electrode is less efficient than the non-coated electrode. The uniformity also suffered for the polymer coating, where Figure 19 showcases an area where copper is at a high intensity. The inability to separate cobalt and nickel at a larger scale, inefficiency in electrodeposition, and uneven deposition make coating the electrode in PDADMA polymer unideal.

Chapter 4: Conclusion

Battery recycling is vital for the creation of a closed loop system for lithium ion batteries as the growth of batteries is expected to increase with the advancement of technologies needing efficient energy storage. Current battery recycling companies utilize pyrometallurgical and hydrometallurgical recycling, with hydrometallurgical recycling being viewed as the most environmentally friendly process. In hydrometallurgical recycling, electrodeposition is investigated as the recovery of choice to reduce hazardous chemicals and separation process complexities present in solvent extraction and chemical precipitation⁴⁷.

Both nickel and cobalt were successfully reduced from ions in solution, simulating a leached NMC lithium ion battery solution. Electrodeposition was done utilizing a galvanostatic current of -0.25 amps at 4900 seconds on an active area of 25 cm² to deposit 0.373 grams of material with an expected ratio of approximately 1 to 1 of cobalt to nickel. Both deposits were higher than the theoretical yield, attributable to the electrolyte saturation of the deposit material and the assumptions made for the theoretical yield.

PDADMA was used to coat the copper working electrode surface to separate cobalt from nickel but was unsuccessful and resulted in similar ratios to a normal copper working electrode. The polymer coating inhibited the electrodeposition of cobalt and resulted in lower yield, fluctuations in voltage, and localized areas where less deposition occurs, revealing the electrode surface. From this experiment, PDADMA is not ideal for a larger scale electrodeposition operation due to the inability to separate the desired elements and providing inefficient reactions.

Despite flaws in separating the individual elements, electrodeposition is still a useful tool for obtaining cobalt and nickel from the leached cathode material to use as either a nickel-cobalt alloy or a precursor to creating new cathode material. The alloy could be either left unchanged,

using its permanent magnetic properties with high communication speed ⁴⁸, or alloyed with other elements to create preexisting alloys that contain cobalt and nickel, such as alnico for commercial magnets ⁴⁹ or Kovar for sealing glass and metal ^{50,51}. For the creation of new cathode material, the electrodeposit would be implemented into preexisting processes that create new batteries from leachate, such as Ascend Elements ¹⁷.

Future works would include investigating cobalt and nickel separation further, testing physical and chemical properties of the deposit material, and creating a battery cathode production process with electrodeposition. Investigating the cobalt and nickel separation would include changing the electrolyte and polymer coating concentrations to determine the fundamental cause of inconsistency between this study and others. Chemical properties of nickel-cobalt alloy electrodeposits have recently been investigated by Liu et al., where the alloy's diffraction peaks correlated to the $\{1\ 1\ 1\}$, $\{2\ 0\ 0\}$, and $\{2\ 2\ 0\}$ facets ⁵². This would be supplemented with testing physical properties to determine the usage of the alloy and its material structure. To include electrodeposition into a production process, the deposit's ratio would be determined and then combined as a precursor to a battery cathode material by adding the additional elements required.

References

1. Yoshino, A. The birth of the lithium-ion battery. *Angewandte Chemie - International Edition* vol. 51 5798–5800 Preprint at <https://doi.org/10.1002/anie.201105006> (2012).
2. Mizushima, K., Jones, P. C., Wiseman, P. J. & Goodenough, J. B. *Li_xCoO₂ (0 < x < 1): A NEW CATHODE MATERIAL FOR BATTERIES OF HIGH ENERGY DENSITY*. *Mat. Res. Bull* vol. 15 (1980).
3. Ozawa, K. *Lithium-ion rechargeable batteries with LiCoO₂ and carbon electrodes: the LiCoO₂/C system*. *Solid State Ionics* vol. 69 (1994).
4. Palacín, M. R. & De Guibert, A. Batteries: Why do batteries fail? *Science* vol. 351 Preprint at <https://doi.org/10.1126/science.1253292> (2016).
5. *Multi-Pollutant Emissions Standards for Model Years 2027 and Later Light-Duty and Medium-Duty Vehicles*. (2023).
6. Harper, G. *et al.* Recycling lithium-ion batteries from electric vehicles. *Nature* vol. 575 75–86 Preprint at <https://doi.org/10.1038/s41586-019-1682-5> (2019).
7. Li, D., Danilov, Dmitri L., Bergveld, H. J., Eichel, R.-A. & Notten, P. H. L. *Understanding Battery Aging Mechanisms*. www.rsc.org (2019).
8. Steckelberg, A., Dormido, H., Mellen, R., Rich, S. & Brown, C. The Underbelly of Electric Vehicles. *Washington Post* (2023).
9. Tsurukawa, N., Prakash, S. & Manhart, A. *Social impacts of artisanal cobalt mining in Katanga, Democratic Republic of Congo Social impacts of artisanal cobalt mining in Katanga, Democratic Republic of Congo III*. (2011).
10. *Cobalt Market Report 2022*. (2023).
11. van den Brink, S., Kleijn, R., Sprecher, B. & Tukker, A. Identifying supply risks by mapping the cobalt supply chain. *Resour Conserv Recycl* **156**, (2020).
12. Chen, M. *et al.* Recycling End-of-Life Electric Vehicle Lithium-Ion Batteries. *Joule* vol. 3 2622–2646 Preprint at <https://doi.org/10.1016/j.joule.2019.09.014> (2019).
13. Gaines, L. The future of automotive lithium-ion battery recycling: Charting a sustainable course. *Sustainable Materials and Technologies* **1**, 2–7 (2014).
14. Jie, Y. *et al.* Oxidizing roasting behavior and leaching performance for the recovery of spent lifepo₄ batteries. *Minerals* **10**, 1–16 (2020).
15. Chagnes, A. & Pospiech, B. A brief review on hydrometallurgical technologies for recycling spent lithium-ion batteries. *Journal of Chemical Technology and Biotechnology* vol. 88 1191–1199 Preprint at <https://doi.org/10.1002/jctb.4053> (2013).

16. Wang, R. C., Lin, Y. C. & Wu, S. H. A novel recovery process of metal values from the cathode active materials of the lithium-ion secondary batteries. *Hydrometallurgy* **99**, 194–201 (2009).
17. Wang, Y., Apelian, D. & Zou, H. Method And Apparatus for Recycling Lithium-Ion Batteries. (2013).
18. Xu, P. *et al.* Efficient Direct Recycling of Lithium-Ion Battery Cathodes by Targeted Healing. *Joule* **4**, 2609–2626 (2020).
19. Rajaeifar, M. A. *et al.* Life cycle assessment of lithium-ion battery recycling using pyrometallurgical technologies. *J Ind Ecol* **25**, 1560–1571 (2021).
20. Kim, K. *et al.* Electrochemical approaches for selective recovery of critical elements in hydrometallurgical processes of complex feedstocks. *iScience* **24**, 102374 (2021).
21. Chernyshova, I., Bakuska, D. & Ponnurangam, S. Selective Recovery of Critical and Toxic Elements from Their Low-Concentrated Solutions Using Surface-Based Electrochemical Separation Methods. in *ACS Symposium Series* vol. 1348 115–165 (American Chemical Society, 2020).
22. Wang, F., Sun, R., Xu, J., Chen, Z. & Kang, M. Recovery of cobalt from spent lithium ion batteries using sulphuric acid leaching followed by solid-liquid separation and solvent extraction. *RSC Adv* **6**, 85303–85311 (2016).
23. Nicol, M., Welham, N. & Senanayake, G. Solvent Extraction. in *Hydrometallurgy* vol. 2 117–170 (2022).
24. Ciez, R. E. & Whitacre, J. F. Examining different recycling processes for lithium-ion batteries. *Nat Sustain* **2**, 148–156 (2019).
25. Barik, S. P., Prabakaran, G. & Kumar, L. Leaching and separation of Co and Mn from electrode materials of spent lithium-ion batteries using hydrochloric acid: Laboratory and pilot scale study. *J Clean Prod* **147**, 37–43 (2017).
26. Gratz, E., Sa, Q., Apelian, D. & Wang, Y. A closed loop process for recycling spent lithium ion batteries. *J Power Sources* **262**, 255–262 (2014).
27. Cui, C. Q., Jiang, S. P. & Tseung, A. C. C. Electrodeposition of Cobalt from Aqueous Chloride Solutions. *Electrochemical Society* (1990).
28. Altimari, P., Schiavi, P. G., Rubino, A. & Pagnanelli, F. Electrodeposition of cobalt nanoparticles: An analysis of the mechanisms behind the deviation from three-dimensional diffusion-control. *Journal of Electroanalytical Chemistry* **851**, (2019).
29. Kim, K., Raymond, D., Candego, R. & Su, X. Selective cobalt and nickel electrodeposition for lithium-ion battery recycling through integrated electrolyte and interface control. *Nat Commun* **12**, (2021).

30. Su, X. & Hatton, T. A. Electrosorption. in *Kirk-Othmer Encyclopedia of Chemical Technology* 1–11 (Wiley, 2016). doi:10.1002/0471238961.koe00022.
31. Liu, X., Wu, J. & Wang, J. Electro-enhanced removal of cobalt ions from aqueous solution by capacitive deionization. *Science of the Total Environment* **697**, (2019).
32. Sadyrbaeva, T. Z. Separation of cobalt(II) from nickel(II) by a hybrid liquid membrane-electrodialysis process using anion exchange carriers. *Desalination* **365**, 167–175 (2015).
33. Mollah, M. Y. A. *et al.* Fundamentals, present and future perspectives of electrocoagulation. *J Hazard Mater* **114**, 199–210 (2004).
34. Shafaei, A., Pajootan, E., Nikazar, M. & Arami, M. Removal of Co (II) from aqueous solution by electrocoagulation process using aluminum electrodes. *Desalination* **279**, 121–126 (2011).
35. Pinna, E. G., Ruiz, M. C., Ojeda, M. W. & Rodriguez, M. H. Cathodes of spent Li-ion batteries: Dissolution with phosphoric acid and recovery of lithium and cobalt from leach liquors. *Hydrometallurgy* **167**, 66–71 (2017).
36. Zante, G., Masmoudi, A., Barillon, R., Trébouet, D. & Boltoeva, M. Separation of lithium, cobalt and nickel from spent lithium-ion batteries using TBP and imidazolium-based ionic liquids. *Journal of Industrial and Engineering Chemistry* **82**, 269–277 (2020).
37. Garcia, E. M., Santos, J. S., Pereira, E. C. & Freitas, M. B. J. G. Electrodeposition of cobalt from spent Li-ion battery cathodes by the electrochemistry quartz crystal microbalance technique. *J Power Sources* **185**, 549–553 (2008).
38. Skilbred, E. S. *Corrosion of Nickel-Aluminium Bronze How does the different alloying elements effect the corrosion properties?* (2016).
39. Fuller, T. F. & Harb, J. N. *Electrochemical Engineering*. (Wiley, 2018).
40. Bjerrum, J., Halonin, A. S. & Skibsted, L. H. Studies on Cobalt(II) Halide Complex Formation. A Spectrophotometric Study of the Chloro Cobalt(II) Complexes in Strong Aqueous Chloride Solutions. *Acta Chemica Scandinavica A* **29**, 326–332 (1975).
41. Wilson Swaddle, T., D Leonard Fabes, A. N. & Fabes, L. Octahedral-tetrahedral equilibria in aqueous cobalt(II) solutions at high temperatures. *Can J Chem* **58**, (1980).
42. Balakiushnan Nambiar, G. & Subbaraman, P. R. *ANION-EXCHANGE SEPARATION OF COBALT FROM NICKEL*. *Talanta* vol. 14 (1967).
43. Williams, D. B. (David B. & Carter, C. Barry. *Transmission electron microscopy : a textbook for materials science*. (Springer, 2009).
44. FitzGerald, S. XRF Analysis. *Horiba Scientific* <https://www.horiba.com/usa/scientific/technologies/energy-dispersive-x-ray-fluorescence-ed-xrf/xrf-analysis/> (2009).

45. Kawai, J., Yamasaki, K. & Tanaka, R. Fundamental Parameter Method in X-Ray Fluorescence Analysis . in *Encyclopedia of Analytical Chemistry* 1–14 (Wiley, 2019). doi:10.1002/9780470027318.a9666.
46. Kikongi, P., Salvas, J. & Gosselin, R. Curve-fitting regression: improving light element quantification with XRF. *X-Ray Spectrometry* **46**, 347–355 (2017).
47. Zhang, X. *et al.* Toward sustainable and systematic recycling of spent rechargeable batteries. *Chemical Society Reviews* vol. 47 7239–7302 Preprint at <https://doi.org/10.1039/c8cs00297e> (2018).
48. Oriňáková, R., Turoňová, A., Kladeková, D., Gálová, M. & Smith, R. M. Recent developments in the electrodeposition of nickel and some nickel-based alloys. *J Appl Electrochem* **36**, 957–972 (2006).
49. Constantinides, S. Permanent magnet coatings and testing procedures. in *Modern Permanent Magnets* 371–402 (Elsevier, 2022). doi:10.1016/B978-0-323-88658-1.00011-X.
50. Ardebili, H., Zhang, J. & Pecht, M. G. Introduction. in *Encapsulation Technologies for Electronic Applications* 1–45 (Elsevier, 2018). doi:10.1016/B978-0-12-811978-5.00001-8.
51. Eagle Alloys. The Uses and Uniqueness of Kovar. *Eagle Alloys* (2017).
52. Liu, G. *et al.* One-step nickel-cobalt alloy electrodeposition from spent lithium-ion battery via synergistic pH adjustment and Mn²⁺ supplementation. *Sep Purif Technol* **314**, (2023).